

See discussions, stats, and author profiles for this publication at: <https://www.researchgate.net/publication/223975360>

# Sol-Flame Synthesis: A General Strategy To Decorate Nanowires with Metal Oxide/Noble Metal Nanoparticles

ARTICLE in NANO LETTERS · APRIL 2012

Impact Factor: 13.59 · DOI: 10.1021/nl300060b · Source: PubMed

---

CITATIONS

22

READS

100

## 5 AUTHORS, INCLUDING:



[Yunzhe Feng](#)

Stanford University

10 PUBLICATIONS 170 CITATIONS

[SEE PROFILE](#)



[In-Sun Cho](#)

Stanford University

87 PUBLICATIONS 1,930 CITATIONS

[SEE PROFILE](#)



[Lili Cai](#)

Stanford University

17 PUBLICATIONS 291 CITATIONS

[SEE PROFILE](#)



[Xiaolin Zheng](#)

Stanford University

53 PUBLICATIONS 3,051 CITATIONS

[SEE PROFILE](#)

# Sol-Flame Synthesis: A General Strategy To Decorate Nanowires with Metal Oxide/Noble Metal Nanoparticles

Yunzhe Feng,<sup>†,§</sup> In Sun Cho,<sup>‡,§</sup> Pratap M. Rao,<sup>‡</sup> Lili Cai,<sup>‡</sup> and Xiaolin Zheng<sup>\*,‡</sup>

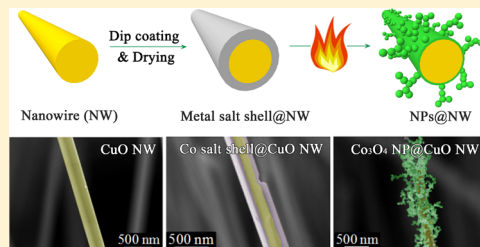
<sup>†</sup>Department of Materials Science and Engineering, Stanford University, Stanford, California 94305, United States

<sup>‡</sup>Department of Mechanical Engineering, Stanford University, Stanford, California 94305, United States

## Supporting Information

**ABSTRACT:** The hybrid structure of nanoparticle-decorated nanowires (NP@NW) combines the merits of large specific surface areas for NPs and anisotropic properties for NWs and is a desirable structure for applications including batteries, dye-sensitized solar cells, photoelectrochemical water splitting, and catalysis. Here, we report a novel *sol-flame* method to synthesize the NP@NW hybrid structure with two unique characteristics: (1) large loading of NPs per NW with the morphology of NP chains fanning radially from the NW core and (2) intimate contact between NPs and NWs. Both features are advantageous for the above applications that involve both surface reactions and charge transport processes. Moreover, the sol-flame method is simple and general, with which we have successfully decorated various NWs with binary/ternary metal oxide and even noble metal NPs. The unique aspects of the sol-flame method arise from the ultrafast heating rate and the high temperature of flame, which enables rapid solvent evaporation and combustion, and the combustion gaseous products blow out NPs as they nucleate, forming the NP chains around NWs.

**KEYWORDS:** Hybrid structure, sol flame, flame synthesis, nanowires, hierarchical structure



The hybrid structure of nanoparticle-decorated nanowire arrays (NP@NW) combines the high aspect ratio and highly controllable structure of an oriented nanowire skeleton<sup>1</sup> with the large surface area of nanoparticles. The electrical, optical, and chemical properties<sup>2</sup> of these hybrid materials can be engineered by controlling the chemical compositions and morphologies of the NPs and NWs independently. As a result, such hybrid materials offer new opportunities to achieve multifunctionality and have shown potential in a wide range of application areas, such as lithium ion batteries,<sup>3–5</sup> gas sensors,<sup>6,7</sup> photoelectrochemical devices,<sup>7–11</sup> and heterogeneous catalysts.<sup>12</sup> For instance, Fe<sub>3</sub>O<sub>4</sub> NPs@Cu NWs as a Li-ion battery anode showed 6 times higher energy density than Fe<sub>3</sub>O<sub>4</sub> NPs@planar Cu due to the larger loading of Fe<sub>3</sub>O<sub>4</sub> NPs on the Cu NWs than on the planar Cu.<sup>5</sup> CdS NPs (as quantum dots, QDs)@TiO<sub>2</sub> nanorod array showed 28.6 times higher photocurrent than that of a bare TiO<sub>2</sub> nanorod array in a photoelectrochemical cell because the CdS NPs can absorb more visible light, and the single crystal TiO<sub>2</sub> nanorods can efficiently separate and transfer photogenerated electrons from CdS NPs to the F-doped SnO<sub>2</sub> (FTO) electrode.<sup>13</sup> Such hybrid structures also increased light absorption by light scattering due to the presence of additional interfaces.<sup>8</sup> Additionally, Co<sub>3</sub>O<sub>4</sub> NPs@CuO NWs exhibited enhanced light absorption than bare CuO NWs and consequently showed 17% higher photocatalytic efficiency for RhB dye degradation under visible-light irradiation than bare CuO NWs.<sup>9</sup> For all these applications, it is highly desirable to synthesize these hybrid NP@NW structures with several simultaneous qualities: high coverage density of

NPs with minimal aggregation, good contact between NPs and NWs, flexible choices of material composition, good morphology control, minimal contamination from processing, and high yield, in a scalable and controllable manner. So far, however, the reported methods to fabricate the NP@NW structures, such as impregnation and deposition–precipitation,<sup>10,11</sup> electrochemical deposition,<sup>5</sup> physical/chemical vapor deposition,<sup>6</sup> self-assembly,<sup>7,14</sup> and thermal growth,<sup>9,15</sup> either require tedious preparation processes and/or expensive equipments or lack control over the size and morphology of the NW and NP building blocks and cannot, therefore, meet the above requirements.

Here, we report a general *sol-flame* method to decorate arrays of NWs with metal oxide or metal NPs in a simple, scalable, and controllable manner. In particular, our sol-flame method decorates NWs with chains of NPs in a hierarchical morphology. The sol-flame method combines the merits of the sol-gel method,<sup>16</sup> dip-coating, and flame spray pyrolysis<sup>17–19</sup> and is schematically illustrated together with corresponding SEM images in Figure 1. First, the target NWs are grown on a substrate (Figure 1A) by using either a bottom-up or top-down method, and the NP precursor made of metal salt solution is prepared by the sol-gel method. Next, the NP precursor solution is coated uniformly over the entire surface of NWs by dip-coating. After drying in air (or N<sub>2</sub>), a metal salt

**Received:** January 5, 2012

**Revised:** March 28, 2012

**Published:** April 11, 2012



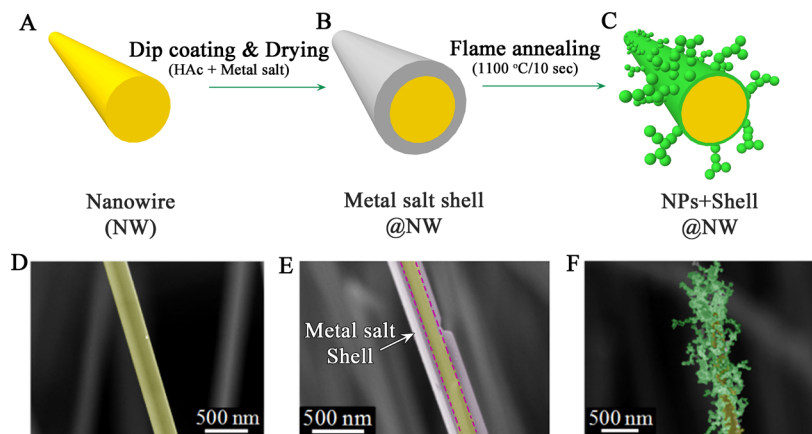


**Figure 1.** Schematic illustration of the general sol-flame synthesis process for hybrid NP@NW nanostructures. The NWs (A) are dip-coated with the precursor solution of NPs and then dried in air (or  $\text{N}_2$ ) to form a metal salt shell on the NWs. Then coated NWs (B) are annealed in the flame, forming a NP-chain morphology (C). The corresponding SEM images of (D)  $\text{CuO}$  NW, (E)  $\text{Co}(\text{CH}_3\text{COO})_2$  shell@ $\text{CuO}$  NW, and (F)  $\text{Co}_3\text{O}_4$  NP@ $\text{CuO}$  NW.

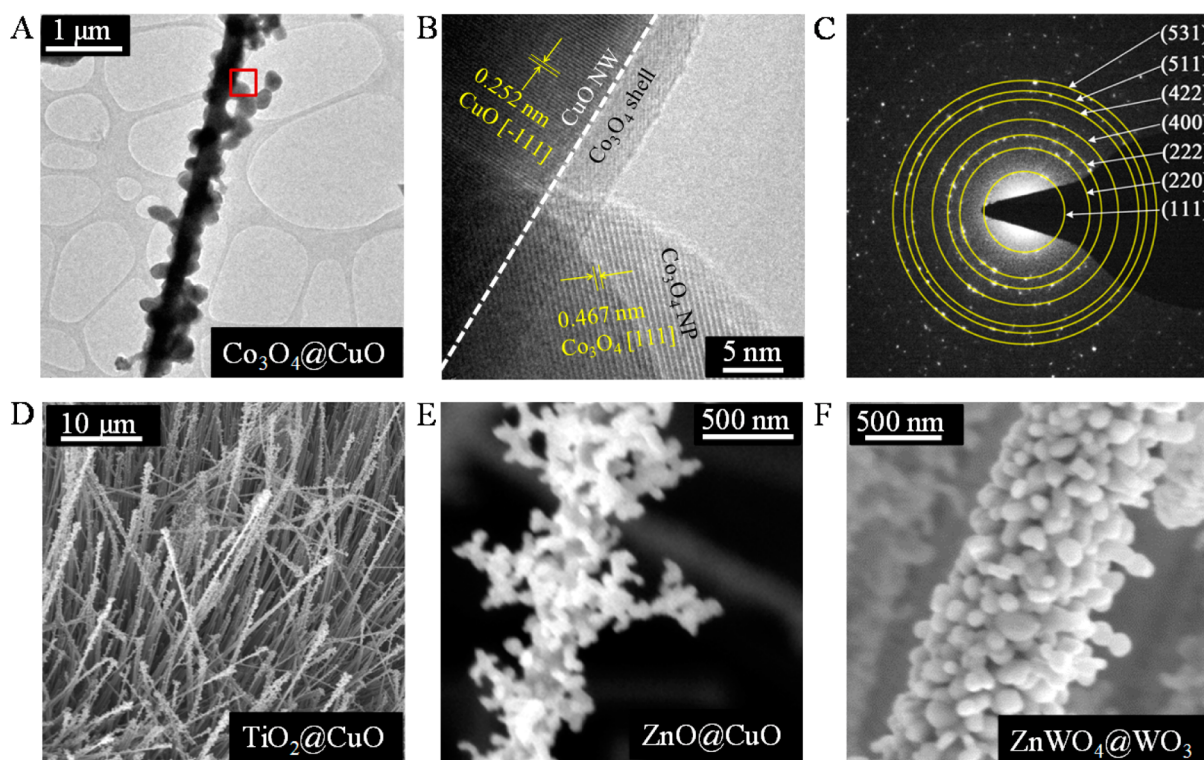


**Figure 2.** (A) TEM (B) HRTEM images and (C) selected area electron diffraction (SAED) pattern of  $\text{Co}_3\text{O}_4$ @ $\text{CuO}$ . All the ring patterns are indexed to cubic spinel  $\text{Co}_3\text{O}_4$ . The HRTEM shows the boxed region in (A). (D–F) SEM images of (D)  $\text{TiO}_2$ @ $\text{CuO}$ , (E)  $\text{ZnO}$ @ $\text{CuO}$ , and (F)  $\text{ZnWO}_4$ @ $\text{WO}_3$ , which were also synthesized by the sol-flame method.

shell is formed on the surface of the NWs (Figure 1B). Finally, the metal salt-coated NWs are annealed over a flame for a few seconds, and consequently the NWs are decorated with a high coverage density of NP chains fanning radially outward from the NW axes (Figure 1C). During the high temperature flame treatment, the remaining solvent in the metal salt shell readily evaporates and combusts, producing gases such as  $\text{H}_2\text{O}$  and  $\text{CO}_2$ <sup>20</sup> that flow radially outward, blowing the metal salt precursors away from the NWs. These metal salt precursors decompose chemically to the final metal or metal oxide composition and nucleate locally, forming the NP chain morphology. Moreover, the high temperature of the flame

and short annealing time lead to high nucleation rate and suppress grain growth and hence ensure small and less aggregated NPs around the NWs (Figure 1C). The short annealing time is facilitated by the fast heating rate of the substrate by the flame. Additionally, the sol-flame method, compared to the traditional flame spray pyrolysis method,<sup>17–19</sup> localizes the coating and nucleation process in the proximity of the target NWs, enabling conformal coating with fine control, and it simplifies the particle deposition process and equipment requirement.

To illustrate the sol-flame method, we have synthesized  $\text{Co}_3\text{O}_4$  NPs on  $\text{CuO}$  NW arrays ( $\text{Co}_3\text{O}_4$ @ $\text{CuO}$ ) grown on a

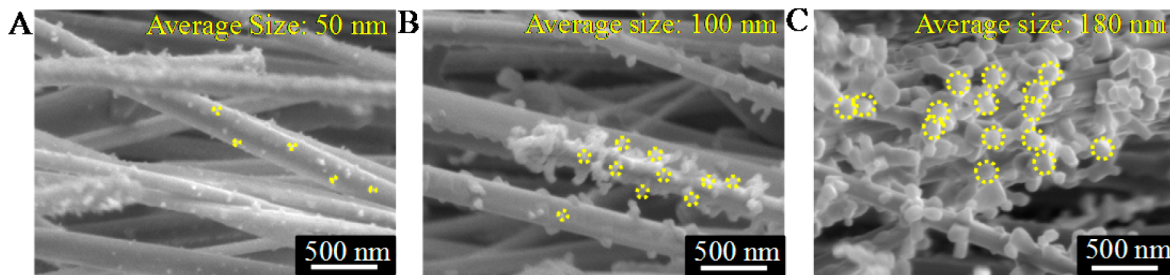


**Figure 3.** Size and coverage density of NPs can be controlled by varying the number of dip-coating. SEM images of  $\text{Co}_3\text{O}_4@\text{CuO}$  synthesized by dip-coating CuO NWs in 0.10 M  $\text{Co}(\text{CH}_3\text{COO})_2$  for (A) 1 time, with an average NP size of 50 nm, (B) 3 times, with an average NP size of 100 nm, and (C) 5 times, with an average NP size of 180 nm. For all the samples, the flame annealing temperature was 1100 °C and annealing duration was 1 min.

Cu mesh substrate. The scanning electron microscope (SEM, FEI XL30 Sirion, 5 kV) images in Figure 1D–F show the CuO NWs at different stages of the synthesis. The CuO NWs were grown by annealing Cu foil at 520 °C in air for 2 days through the solid diffusion mechanism (Figure 1D).<sup>21–23</sup> The as-grown CuO NWs were first coated with a thin layer of cobalt salt shell after the dip-coating step (Figure 1E and Figure S1), and the thin layer was transformed to  $\text{Co}_3\text{O}_4$  NP chains after the flame annealing (Figure 1F). The  $\text{Co}_3\text{O}_4@\text{CuO}$  was further examined using a transmission electron microscope (TEM, Philips CM20 FEG, 200 kV, Figure 2A). The diameter of the  $\text{Co}_3\text{O}_4$  NPs is about 100 nm, and the particles uniformly cover the surface of the CuO NW. These  $\text{Co}_3\text{O}_4$  NPs clearly nucleate as individual NPs without agglomeration into large particles, which is a highly desired feature for materials requiring large surface areas, such as catalysts.<sup>24,25</sup> The interface between NWs and NPs marked in the boxed region of Figure 2A was further characterized by a high-resolution TEM (HRTEM), as shown in Figure 2B. The CuO NW is single crystal with a [111] growth direction and the attached  $\text{Co}_3\text{O}_4$  NP is also highly crystalline. Interestingly, there is a thin  $\text{Co}_3\text{O}_4$  layer of ~4 nm thickness between the CuO NWs and  $\text{Co}_3\text{O}_4$  NPs, which would ensure good electrical contact and charge transport between the NPs and NWs in applications such as lithium ion batteries.<sup>5</sup> The phase homogeneity and crystallinity of the NP chains are further confirmed by the selected area electron diffraction (SAED) pattern (Figure 2C).

Beyond the example of  $\text{Co}_3\text{O}_4$  NPs@CuO NWs, the sol-flame method is a general method to decorate various metal oxide NWs with diverse binary metal oxide NPs through the independent selection of the NWs and the NP precursors.  $\text{TiO}_2$  (Figure 2D),  $\text{ZnO}$  (Figure 2E), and  $\text{NiO}$  NP (Figure S4) chains were respectively deposited onto CuO NW arrays on a copper mesh with the sol-flame method, and the HRTEM images in Figures S2–4 show that all these binary oxide NPs are single crystalline. It should be noted that when the NP and the NW tend to form stable complex, the formed NPs can be ternary oxide NPs formed by additional reactions between the NPs and NWs during the flame annealing step. For example, single crystal  $\text{ZnWO}_4$  NPs<sup>26</sup> were formed on  $\text{WO}_3$  NW arrays ( $\text{ZnWO}_4@\text{WO}_3$ ) when zinc salt-coated  $\text{WO}_3$  NWs<sup>27</sup> were annealed in flame for 1 min (Figure 2F and Figures S5A–C show the corresponding HRTEM image as well as SAED and XRD patterns). Similarly,  $\text{CoWO}_4@\text{WO}_3$ <sup>28</sup> (Figure S6) and  $\text{Fe}_2\text{O}_3/\text{Cu}_{x}\text{Fe}_{3-x}\text{O}_4@\text{CuO}$ <sup>29</sup> (Figure S7) were synthesized by annealing Co salt-coated  $\text{WO}_3$  and Fe salt-coated CuO NW arrays in flame, respectively. All these cases share common characteristics of (1) uniform and dense coverage of NP chains

on NWs with a thin shell of the NP material covering the NWs first, (2) uniform particle decoration over the entire NW growth substrate, and (3) highly crystalline and minimally aggregated NPs.

Our limited study shows that the sol-flame method offers control, though not precisely, over the size and coverage density of the NPs through control of the metal salt precursor concentration, the number of dip coats, the flame annealing temperature, and the annealing duration. The NP size can be varied from tens to hundreds of nanometers, and the number of NPs per micrometer of NW can range from tens to hundreds. For example, increasing the number of dip coats increases the metal salt loading on the NW surface, leading to larger and more densely arranged NPs. Figure 3 illustrates  $\text{Co}_3\text{O}_4@\text{CuO}$  structures for which the CuO NWs were dipped into the 0.1 M Co salt solution 1 time (Figure 3A), 3 times (Figure 3B), and 5 times (Figure 3C). The average size of the  $\text{Co}_3\text{O}_4$  NPs increases with the number of dip coats, with diameters of 50, 100, and 180 nm for 1 time, 3 times, and 5 times dip-coating, respectively. Simultaneously, the coverage density of the  $\text{Co}_3\text{O}_4$  NPs also increases from sparse to dense coverage with the increasing number of coats. Besides the number of dip coats, the effects of other experimental parameters, i.e., the solution concentration, the flame annealing temperature, and annealing duration, on the size and coverage density of NPs were also studied, as shown in Figure S10. Increasing the metal salt concentration in the initial sol solution results in larger NP size and higher coverage density because more metal salt is coated on the surface of NWs (similar effect to the number of dip-coats). Additionally, the NP coverage density can be independently changed with respect to the NP size by applying dip-coating and flame annealing process for multi-times. However, neither the flame annealing temperature (as long as it is above 600 °C) nor the annealing duration (in the range of 5 s to 1 min) had significant effects on the size or coverage density of the final NPs. Such insensitivity allows the sol-flame method to be carried out without strict restrictions on the flame treatment conditions.

Notably, the sol-flame method can be used to decorate metal oxide NWs with more complicated ternary metal oxide or even noble metal NPs. The ternary oxide NP case is realized by mixing two different metal salt precursors together in the initial sol solution. Specifically, by dip-coating CuO NWs in an Fe and Co salt mixture solution (atomic ratio of Fe:Co is 1:14) and annealing them in a flame, ternary iron–cobalt oxide ( $\text{Fe}_x\text{Co}_{3-x}\text{O}_4$ ,  $x \sim 0.2$ ) NPs on CuO NW arrays ( $\text{Fe}_x\text{Co}_{3-x}\text{O}_4@\text{CuO}$ ) were formed. The TEM image of  $\text{Fe}_x\text{Co}_{3-x}\text{O}_4@\text{CuO}$  (Figure 4A) shows that  $\text{Fe}_x\text{Co}_{3-x}\text{O}_4$  NPs

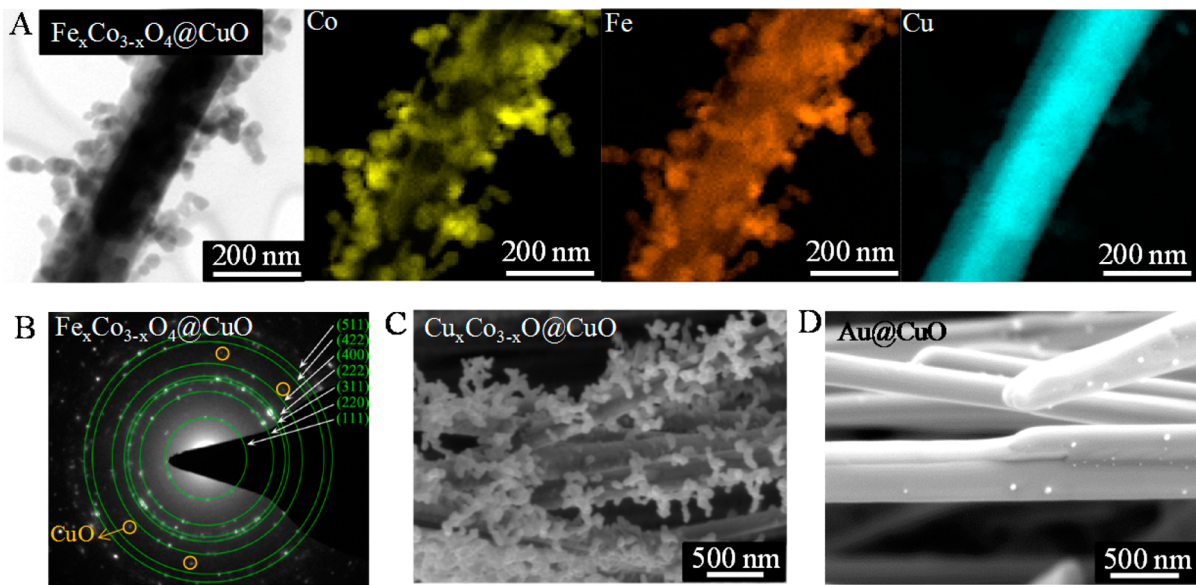


**Figure 4.** (A) TEM image of  $\text{Fe}_x\text{Co}_{3-x}\text{O}_4@\text{CuO}$  ( $x \sim 0.2$ ) NWs and the corresponding TEM-EDS elemental mapping of Co, Fe, and Cu. (B) SAED pattern of  $\text{Fe}_x\text{Co}_{3-x}\text{O}_4@\text{CuO}$  ( $x \sim 0.2$ ) NWs and all the ring patterns are indexed to be spinel structure. SEM images of (C)  $\text{Cu}_x\text{Co}_{3-x}\text{O}@\text{CuO}$  ( $x \sim 0.2$ ) NWs and (D) Au@CuO NWs, which were also synthesized by the sol-flame method.

with an average diameter of 50 nm are uniformly and densely decorated on the CuO NWs with a chain morphology similar to that of the binary metal oxide NPs (Figure 2). TEM energy dispersive X-ray spectroscopy (EDS) analysis (Figure 4A) shows that the NPs contain uniformly distributed Co and Fe and Cu is mainly contained in the NW core region with a smaller amount existing in the NPs as well, indicating that some CuO was dissolved by the acetic acid in the sol–gel solution during the dip-coating process. The formation of  $\text{Fe}_x\text{Co}_{3-x}\text{O}_4$  is further confirmed by the SAED patterns for which all the rings are indexed to cubic spinel structure (Figure 4B). Similarly, other ternary oxide NPs of  $\text{Cu}_x\text{Co}_{3-x}\text{O}_4$  ( $x \sim 0.2$ , Figure 4C and Figure S8) and  $\text{Zn}_x\text{Fe}_{3-x}\text{O}_4$  ( $x \sim 1$ , Figure S9) were also successfully synthesized on CuO NW arrays by the sol-flame method. Significantly, in addition to ternary oxides, Au NPs were decorated onto CuO NWs by the same sol-flame method. As shown in Figure 4D, the NPs with an average diameter of 15 nm were uniformly distributed on the surface of the CuO NWs. The ability to decorate ternary oxides and noble metal NPs on NWs greatly increases the chemical tunability and material choice in the final hybrid structured NP@NW and thus expands their potential application areas.

Finally, the major merit of this sol-flame method comes from the flame annealing step, which provides an ultrafast heating rate and short annealing time. To demonstrate the importance of the ultrafast heating rate in forming the NP chain morphology, ZnO NPs@CuO NWs were annealed by three different methods, starting at room temperature, after dip-coating the Zn precursor solution: (1) furnace annealing at 850 °C for 1 h, with a slow heating rate of 5 °C/min from room temperature, (2) furnace annealing at 850 °C for 1 min, with a fast heating rate of ~1000 °C/min obtained by inserting the samples directly into a hot furnace at 850 °C, and (3) flame annealing at 1100 °C for 1 min, with an ultrafast heating rate of ~10 000 °C/min obtained by inserting samples directly into the flame. The flame heating rate is very large because of the large convective flow velocity in the flame and due to radiation from the flame. Since the morphology of NPs synthesized by

the sol-flame method is insensitive to flame annealing temperature above 600 °C, the flame annealing temperature of 1100 °C is typical and representative of all temperatures above 600 °C. As such, flame annealing at 1100 °C can be directly compared to furnace annealing at 850 °C. As shown in Figure S11, for the furnace annealing case with slow heating rate, large ZnO particles with sizes in the range of 500–700 nm were formed on the CuO NWs, whereas for the furnace annealing with a faster heating rate, small ZnO NPs with sizes in the range of 80–160 nm were formed uniformly on the CuO NWs. Interestingly, the deposited ZnO NPs (with sizes in the range of 50–150 nm) formed a NP-chain morphology only in the flame annealing case. This is because both the furnace annealing methods allow a long time for the solvent in the coated shell to evaporate gradually (Figure 1B) before the metal salt decomposes. Hence, the metal salts decompose and nucleate densely within the shell to form closely packed grains that then coalesce and grow, resulting in densely coated, large particles. In contrast, for the fast flame annealing case, the solvent is quickly evaporated and combusted, and the gaseous combustion products blow off the NP precursors, which nucleate while being radially ejected from the NWs, forming the NP-chain morphology.<sup>20</sup> Furthermore, the NWs were only briefly exposed (several seconds) to the high temperature flame during the treatment, so we found that even delicate substrates such as fluorine-doped tin oxides (FTO) can be used to host NWs without the risk of substrate damage. To demonstrate the merits of flame annealing, we annealed Co salt-coated  $\text{WO}_3$  NWs (grown on FTO substrate) in flame (1100 °C, 1 min) and furnace (450 °C, 30 min) that lead to the formation of  $\text{CoWO}_4@\text{WO}_3$  and  $\text{Co}_3\text{O}_4@\text{WO}_3$ , respectively, due to the treatment temperature difference. The furnace annealing temperature was kept low to protect the FTO substrate from damaging. We further compared the catalytic activities of the bare  $\text{WO}_3$ , the furnace-annealed  $\text{Co}_3\text{O}_4@\text{WO}_3$ , and the flame-annealed  $\text{CoWO}_4@\text{WO}_3$  for the oxygen evolution reaction (OER) (Figure S12A), and their corresponding current densities ( $J$ ) at 2.5 V vs RHE are 0.42, 4.05, and 8.64 mA/

$\text{cm}^2$ , respectively. First, both  $\text{Co}_3\text{O}_4@\text{WO}_3$  and  $\text{CoWO}_4@\text{WO}_3$  samples show much higher  $J$  values than the bare  $\text{WO}_3$ , demonstrating the merits of hybrid structures in modifying surface chemistry. Second, although the catalytic activity of  $\text{CoWO}_4$  for OER is lower than that of  $\text{Co}_3\text{O}_4$ ,<sup>30</sup> the flame-annealed  $\text{CoWO}_4@\text{WO}_3$  still exhibits twice higher  $J$  values than that of the furnace-annealed  $\text{Co}_3\text{O}_4@\text{WO}_3$ , indicating that the flame-annealed sample has a much larger surface area. Finally, the flame-annealed  $\text{CoWO}_4@\text{WO}_3$  exhibits comparable stability to that of furnace-annealed sample during the 550 s measurement (Figure S12B). Therefore, the sol-flame method enables the modification of NWs with chemically active NPs with large loading and hence large surface area, which is desirable for many applications requiring large surface areas, such as catalysis, gas sensors, and photoelectrochemical devices.

To summarize, we have developed a general *sol-flame* method to decorate arrays of metal oxide NWs with highly crystalline NPs. With this sol-flame method, we have demonstrated three different types of NP@NW hybrid structures (summarized in Table S1): (1) binary metal oxide NP@NW, including  $\text{Co}_3\text{O}_4@\text{CuO}$ ,  $\text{TiO}_2@\text{CuO}$ ,  $\text{ZnO}@\text{CuO}$ , and  $\text{NiO}@\text{CuO}$ ; (2) ternary metal oxides NP@NW, including  $\text{ZnWO}_4@\text{WO}_3$ ,  $\text{CoWO}_4@\text{WO}_3$ ,  $\text{Fe}_2\text{O}_3/\text{Cu}_x\text{Fe}_{3-x}\text{O}_4@\text{CuO}$ ,  $\text{Fe}_x\text{Co}_{3-x}\text{O}_4@\text{CuO}$  ( $x \sim 0.2$ ),  $\text{Cu}_x\text{Co}_{3-x}\text{O}_4@\text{CuO}$  ( $x \sim 0.2$ ), and  $\text{Zn}_x\text{Fe}_{3-x}\text{O}_4@\text{CuO}$  ( $x \sim 1$ ); and (3) noble metal NP@NW, such as  $\text{Au}@\text{CuO}$ . Notably, both the size and the coverage density of the NPs can be controlled to a certain degree by varying the concentration of the initial precursor solution and the number of dip-coated layers, and further research is needed for achieving more precise morphology control of NPs. The unique aspects of the sol-flame method are the ultrafast heating rate and high temperature of the flame, which enable rapid solvent evaporation and combustion, and nucleation of NPs in the vicinity of the NWs without significant NP agglomeration, leading to the unique NP chain morphology on NWs. Additionally, a thin layer of the NP material is also formed between the NPs and NWs for some cases, which ensures the intimate contact and strong attachment of the NPs to the NWs. Given the generality and versatility of the sol-flame method, we believe it will enable the synthesis of various interesting NP@NW hybrid structures and thereby have an impact on diverse technologies such as lithium ion batteries, catalysts, and photoelectrochemical devices.

**Experimental Methods.** *Preparation of the CuO NW Arrays.* The CuO NWs were grown by the thermal annealing method.<sup>21–23</sup> Briefly, a piece of copper mesh (mesh density:  $100 \times 100 \text{ in.}^{-2}$ ; wire diameter: 0.0045 in.; McMaster) with dimensions of  $1 \text{ cm} \times 1 \text{ cm}$  was annealed in air inside a tube furnace at  $520^\circ\text{C}$  for 2 days. CuO NWs were formed perpendicularly to the copper mesh surface with a diameter range of  $100\text{--}200 \text{ nm}$  and an average length of  $50 \mu\text{m}$ .

*Preparation of  $\text{WO}_3$  NW Arrays.* The  $\text{WO}_3$  nanowires were synthesized by flame vapor deposition.<sup>27,31,32</sup> First, substoichiometric  $\text{W}_{18}\text{O}_{49}$  ( $\text{WO}_{2.72}$ ) nanowires were synthesized by evaporating  $\text{WO}_x$  vapor onto stainless steel (SS) wire mesh or FTO substrates in a flame for 30 min. Specifically, W wire meshes placed above a premixed  $\text{CH}_4$ -air flame are oxidized and evaporated by the hot flame product gases at temperatures of  $\sim 1000^\circ\text{C}$  to generate  $\text{WO}_x$  vapors that are carried downstream and deposit onto the colder growth substrate. The temperature of the growth substrate was kept at  $600^\circ\text{C}$  by a water-cooled plate at the backside of the substrate. Finally, the

as-grown  $\text{W}_{18}\text{O}_{49}$  nanowires were further oxidized to  $\text{WO}_3$  at  $550^\circ\text{C}$  for 2 h in air.

*Preparation of the Sol-Gel Solution.* The precursor solutions of  $\text{ZnO}$ ,  $\text{Co}_3\text{O}_4$ ,  $\text{TiO}_2$ ,  $\text{NiO}$ ,  $\text{Fe}_2\text{O}_3$ ,  $\text{Fe}_x\text{Co}_{3-x}\text{O}_4$  ( $x \sim 0.2$ ),  $\text{Cu}_x\text{Co}_{3-x}\text{O}_4$  ( $x \sim 0.2$ ), and  $\text{Zn}_x\text{Fe}_{3-x}\text{O}_4$  ( $x \sim 1$ ) and Au, with a typical total metal salt concentration of 0.02–0.1 M, were prepared by mixing their corresponding metal salts ( $\text{Zn}(\text{CH}_3\text{COO})_2 \cdot 2\text{H}_2\text{O}$ , 99%;  $\text{Co}(\text{CH}_3\text{COO})_2 \cdot 4\text{H}_2\text{O}$ , 99%;  $\text{Ti}[\text{OCH}(\text{CH}_3)_2]_4$ , 97%;  $\text{Ni}(\text{CH}_3\text{COO})_2 \cdot 4\text{H}_2\text{O}$ , 99%;  $\text{Fe}(\text{NO}_3)_3 \cdot 9\text{H}_2\text{O}$ , 98%;  $\text{Cu}(\text{CH}_3\text{COO})_2 \cdot \text{H}_2\text{O}$ , >99%;  $\text{AuCl}_3$ , 99%; Sigma-Aldrich Chemicals) with acetic acid ( $\text{CH}_3\text{COOH}$ , 99.7%, EMD Chemicals). For the ternary compounds solutions, 0.1–0.3 mL of acetylacetone ( $\text{CH}_3\text{COCH}_2\text{COCH}_3$ , 99%, Sigma-Aldrich Chemicals) was added for the stability of the precursor solution.

*Dip-Coating.* The prepared metal salt solutions were aged for 12 h at room temperature and then used for dip-coating. Prior to the dip-coating, the NW ( $\text{CuO}$  and  $\text{WO}_3$ ) substrates were washed by isopropyl alcohol or ethanol to improve the coating quality/wetting ability of the precursor solutions. The cleaned NWs substrates were then dipped into the metal salt solution and withdrawn vertically at a constant speed (1.0 mm/s). Finally, the coated NW substrates were dried in air or  $\text{N}_2$ .

*Flame Treatment.* The flame annealing was conducted with a premixed coflow flat-flame burner (McKenna Burner) operating on  $\text{CH}_4$  and  $\text{H}_2$  fuels, with air as the oxidizer. The typical flow rates of  $\text{CH}_4$ ,  $\text{H}_2$ , and air were 2.00, 4.00, and 36.7 SLPM, respectively. The metal salt-coated NW substrate was inserted into the postflame region. The typical flame annealing temperature was measured by a K-type thermocouple (1/16 in. bead size, Omega Engineering, Inc.) to be  $1100^\circ\text{C}$ . The typical treatment time was 1 min.

## ASSOCIATED CONTENT

### S Supporting Information

More detailed characterization of the NP@NW structure, controlled experiments, and application of the NP@NW in this work. This material is available free of charge via the Internet at <http://pubs.acs.org.org>.

## AUTHOR INFORMATION

### Corresponding Author

\*E-mail: xlzheng@stanford.edu.

### Author Contributions

<sup>§</sup>These authors contributed equally to this work.

### Notes

The authors declare no competing financial interest.

## ACKNOWLEDGMENTS

This work is supported by the ONR/PECASE program. I.S.C. acknowledges support from the National Research Foundation of Korea Grant funded by the Korean Government (Ministry of Education, Science and Technology) [NRF-2010-357-D00126]. P.M.R. acknowledges support from the Link Foundation Energy Fellowship.

## REFERENCES

- (1) Xia, Y. N.; Yang, P. D.; Sun, Y. G.; Wu, Y. Y.; Mayers, B.; Gates, B.; Yin, Y. D.; Kim, F.; Yan, Y. Q. *Adv. Mater.* **2003**, *15* (5), 353–389.
- (2) Wang, Z. L.; Wang, X.; Sun, X.; Xu, J.; Li, Y. Nanowires and Nanotubes of Complex Oxides Nanowires and Nanobelts. In

Nanowires and Nanobelts: Materials, Properties and Devices; Springer: New York, 2003; Vol. 2, pp 173–190.

(3) Zhou, W.; Cheng, C.; Liu, J.; Tay, Y. Y.; Jiang, J.; Jia, X.; Zhang, J.; Gong, H.; Hng, H. H.; Yu, T.; Fan, H. *J. Adv. Funct. Mater.* **2011**, *21* (13), 2439–2445.

(4) Zhou, S.; Liu, X.; Wang, D. *Nano Lett.* **2010**, *10* (3), 860–863.

(5) Taberna, P. L.; Mitra, S.; Poizot, P.; Simon, P.; Tarascon, J. M. *Nat. Mater.* **2006**, *5* (7), 567–573.

(6) Dobrokhotov, V. V.; McIlroy, D. N.; Norton, M. G.; Abdelrahman, R.; Safir, A.; Berven, C. A. *Nanotechnology* **2009**, *20* (13), 135504.

(7) Zhang, Y.; Xu, J.; Xu, P.; Zhu, Y.; Chen, X.; Yu, W. *Nanotechnology* **2010**, *21* (28), 285501.

(8) Bierman, M. J.; Jin, S. *Energy Environ. Sci.* **2009**, *2* (10), 1050–1059.

(9) Shi, W.; Chopra, N. *J. Nanopart. Res.* **2011**, *13* (2), 851–868.

(10) Lin, C.-H.; Chao, J.-H.; Liu, C.-H.; Chang, J.-C.; Wang, F.-C. *Langmuir* **2008**, *24* (17), 9907–9915.

(11) Tak, Y.; Hong, S. J.; Lee, J. S.; Yong, K. *Cryst. Growth Des.* **2009**, *9* (6), 2627–2632.

(12) Chen, X. H.; Moskovits, M. *Nano Lett.* **2007**, *7* (3), 807–812.

(13) Wang, H.; Bai, Y.; Zhang, H.; Zhang, Z.; Li, J.; Guo, L. *J. Phys. Chem. C* **2010**, *114* (39), 16451–16455.

(14) Xie, Y.; Ding, K.; Liu, Z.; Tao, R.; Sun, Z.; Zhang, H.; An, G. *J. Am. Chem. Soc.* **2009**, *131* (19), 6648–6649.

(15) Lin, Y.; Baggett, D. W.; Kim, J.-W.; Siochi, E. J.; Connell, J. W. *ACS Appl. Mater. Interfaces* **2011**, *3* (5), 1652–1664.

(16) Hench, L. L.; West, J. K. *Chem. Rev.* **1990**, *90* (1), 33–72.

(17) Madler, L.; Kammler, H. K.; Mueller, R.; Pratsinis, S. E. *J. Aerosol Sci.* **2002**, *33* (2), 369–389.

(18) Strobel, R.; Baiker, A.; Pratsinis, S. E. *Adv. Powder Technol.* **2006**, *17* (S), 457–480.

(19) Teoh, W. Y.; Amal, R.; Madler, L. *Nanoscale* **2010**, *2* (8), 1324–1347.

(20) Strobel, R.; Pratsinis, S. E. *Phys. Chem. Chem. Phys.* **2011**, *13* (20), 9246–9252.

(21) Feng, Y.; Zheng, X. *Nano Lett.* **2010**, *10* (11), 4762–4766.

(22) Jiang, X. C.; Herricks, T.; Xia, Y. N. *Nano Lett.* **2002**, *2* (12), 1333–1338.

(23) Feng, Y.; Rao, P. M.; Kim, D. R.; Zheng, X. *Proc. Combust. Inst.* **2010**, *33* (2), 3169–3175.

(24) Choudhary, T. V.; Banerjee, S.; Choudhary, V. R. *Appl. Catal., A* **2002**, *234* (1–2), 1–23.

(25) Marion, M. C.; Garbowski, E.; Primet, M. *J. Chem. Soc., Faraday Trans.* **1990**, *86* (17), 3027–3032.

(26) Shchenev, A. V.; Kargin, Y. F.; Skorikov, V. M. *Russ. J. Inorg. Chem.* **1988**, *33*, 1237–1238.

(27) Rao, P. M.; Zheng, X. *Proc. Combust. Inst.* **2011**, *33* (2), 1891–1898.

(28) French, G. J.; Sale, F. R. *J. Mater. Sci.* **1985**, *20* (4), 1291–1300.

(29) Prince, E.; Treuting, R. G. *Acta Crystallogr.* **1956**, *9* (12), 1025–1028.

(30) Yamada, Y.; Yano, K.; Hong, D.; Fukuzumi, S. *Phys. Chem. Chem. Phys.* **2012**, *14*, 5753–5760.

(31) Cai, L.; Rao, P. M.; Zheng, X. *Nano Lett.* **2011**, *11* (2), 872–877.

(32) Rao, P. M.; Zheng, X. L. *Nano Lett.* **2009**, *9* (8), 3001–3006.